Advances in Nano Research, *Vol. 13, No.3 (2022) 259-267*
https://doi.org/10.12989/anr.2022.13.3.259

Crossover from weak anti-localization to weak localization in inkjet-printed $Ti_3C_2T_x$ MXene thin-film

Mi-Jin Jin[1,2], Doo-Seung Um[*3,4], Osarenkhoe Ogbeide[3], Chang-Il Kim[5], Jung-Woo Yoo[6] and J. W. A. Robinson[**1]

[1]*Department of Materials Science & Metallurgy, University of Cambridge, Cambridge CB3 0FS, United Kingdom*
[2]*Center for Multidimensional Carbon Materials (CMCM), Institute for Basic Science (IBS), Ulsan 44919, Republic of Korea*
[3]*Cambridge Graphene Centre, University of Cambridge, Cambridge CB3 0FA, United Kingdom*
[4]*Department of Electrical Engineering, Sejong University, Seoul 05006, Republic of Korea*
[5]*School of Electrical and Electronics Engineering, Chung-Ang University, Seoul 06974, Republic of Korea*
[6]*Materials Science and Engineering, Ulsan National Institute of Science and Technology (UNIST), Ulsan 44919, Republic of Korea*

(*Received February 3, 2022, Revised August 5, 2022, Accepted August 5, 2022*)

Abstract. Two-dimensional (2D) transition metal carbides/nitrides or "MXenes" belong to a diverse-class of layered compounds, which offer composition- and electric-field-tunable electrical and physical properties. Although the majority of the MXenes, including $Ti_3C_2T_x$, are metallic, they typically show semiconductor-like behaviour in their percolated thin-film structure; this is also the most common structure used for fundamental studies and prototype device development of MXene. Magnetoconductance studies of thin-film MXenes are central to understanding their electronic transport properties and charge carrier dynamics, and also to evaluate their potential for spin-tronics and magnetoelectronics. Since MXenes are produced through solution processing, it is desirable to develop deposition strategies such as inkjet-printing to enable scale-up production with intricate structures/networks. Here, we systematically investigate the extrinsic negative magnetoconductance of inkjet-printed $Ti_3C_2T_x$ MXene thin-films and report a crossover from weak anti-localization (WAL) to weak localization (WL) near 2.5 K. The crossover from WAL to WL is consistent with strong, extrinsic, spin-orbit coupling, a key property for active control of spin currents in spin-orbitronic devices. From WAL/WL magnetoconductance analysis, we estimate that the printed MXene thin-film has a spin orbit coupling field of up to 0.84 T at 1.9 K. Our results and analyses offer a deeper understanding into microscopic charge carrier transport in $Ti_3C_2T_x$, revealing promising properties for printed, flexible, electronic and spin-orbitronic device applications.

Keywords: inkjet printing; magneto-conductance; MXenes; $Ti_3C_2T_x$ network; weak anti-localization (WAL); weak localization (WL)

1. Introduction

MXenes are a new family of the two-dimensional (2D) layered materials with potential for electronic, magnetic, and optical applications due to their tunable band structure and work function through surface functionalization (Anasori *et al.* 2015, 2017, Ghidiu *et al.* 2014, Guo *et al.* 2019, Khazaei *et al.* 2013, Naguib *et al.* 2011, Naguib *et al.* 2012, Soundiraraju *et al.* 2017, Urbankowski *et al.* 2016, VahidMohammadi *et al.* 2021). Over 100 discrete MXenes have been theoretically predicted by combining different transition metals with carbon and/or nitrogen, offering a wide range of applications in addition to fundamental studies (Anasori *et al.* 2015, Dahlqvist *et al.* 2020, Deysher *et al.* 2020, Guo *et al.* 2019, Soundiraraju *et al.* 2017). There are currently over 30 different MXenes with electrical conductivities that vary from metallic to semiconducting behaviour (Enyashin *et al.* 2012, Gao *et al.* 2016, Han *et al.* 2020, Khazaei *et al.* 2013, 2016, 2017, Naguib *et al.* 2011, Xie *et al.* 2013, Zha *et al.* 2015), with theoretical band gaps between 0.05 ~ 2.0 eV (Khazaei *et al.* 2013, Naguib *et al.* 2011). Some of these compositions represent exotic states such as topological insulator behaviour (Fashandi *et al.* 2015, Khazaei *et al.* 2016, Weng *et al.* 2015), ferromagnetism, and antiferromagnetism with high spin-orbit interaction (SOI) (Enyashin *et al.* 2012, Jiang *et al.* 2020, Khazaei *et al.* 2013, Kumar *et al.* 2017, Lang *et al.* 2013, Si *et al.* 2015). Additionally, density-functional theory (DFT) calculations predict that MXenes can exhibit strong spin-orbit coupling at low temperatures for spintronic and spin-orbitronic applications (Chandrasekaran *et al.* 2017, Khazaei *et al.* 2016).

Since MXenes are typically produced from selective etching of their parent MAX phases in an aqueous environment, they have −OH, −O, and −F terminations, rendering them hydrophilic and readily dispersible in many solvents (Akuzum *et al.* 2018, Liu *et al* 2021, Maleski *et al.* 2017). Inkjet printing, spray coating, and vacuum filtration are most widely used deposition techniques for MXene prototype device fabrication from their liquid dispersions

*Corresponding author, Assistant Professor,
E-mail: dsum@sejong.ac.kr
**Co-corresponding author, Professor,
E-mail: jjr33@cam.ac.uk

ISSN: 2287-237X (Print), 2287-2388 (Online)

(Akuzum *et al.* 2018, Maleski *et al.* 2017, Naguib *et al.* 2011, Salles *et al.* 2019, Sarycheva *et al.* 2018). The deposited MXene sheets are randomly stacked, forming a disordered network, which defines the electronic properties of the resultant thin-films. Therefore, it is very important to understand the influence of randomly oriented networks on the charge carrier transport properties of MXene sheets. Recently, Halim *et al.* reported electrical transport of Ti_2CT_x, Nb_2CT_x, $Ti_3C_2T_x$, and Mo_2CT_x MXenes by measuring the temperature- and magnetic-field-dependence of electrical resistance (Anasori *et al.* 2016, Deysher *et al.* 2020, Halim *et al.* 2014, Halim *et al.* 2016, 2019, Pinto *et al.* 2020). It is shown that certain compositions of MXene only exhibit weak localization (WL) around zero magnetic field, indicating that those compositions may not have strong sufficient spin-orbit coupling (Halim *et al.* 2014, 2016, 2019, 2018) to observe weak antilocalization (WAL). Anasori *et al.* (2016) reported carrier transport on $Ti_3C_2T_x$ and $Mo_2TiC_2T_x$ versus temperature and magnetic field with positive and negative magnetoresistance behaviour by substituting the outer Ti with Mo (Anasori *et al.* 2016); however, these reports do not show a detailed analysis of the magnetic field dependence of the electrical resistance (or conductance) of the MXene thin-films in the WAL/WL regimes.

WL and WAL are quantum phenomenon seen in disordered metal or semiconductor systems which exhibit (quantum) diffusive transport at low temperatures (Datta 1995, Heikkilä *et al.* 2013, Liu *et al.* 2017). WL is considered a precursor to strong localization (SL). At low temperatures, quantum diffusive transport in the absence of time-reversal symmetry causes electrons to propagate in a circular path rather than randomly scattering in all directions, producing an increase in the resistivity. Such quantum diffusive transport is disrupted by applying a magnetic field. The delocalization of electrons in materials with strong spin-orbit coupling induces destructive quantum interference of time-reversal loops formed by quantum scattering (Drouhin *et al.* 2014, Liu *et al.* 2017). Therefore, WAL (WL) enhances (suppresses) the conductivity near zero magnetic field. Understanding the WAL/WL behaviour in materials or systems such as MXenes is critical for their development in quantum devices (Caviglia *et al.* 2014, Schmidt *et al.* 2016).

Here, we report extrinsic negative magneto-conductance and a crossover between from WL to WAL at low temperature in a $Ti_3C_2T_x$ MXene thin-film, fabricated by inkjet printing using a mixed solvent functional ink. To determine the carrier mobility of MXene, the MXene sheets are inkjet-printed into a 'Hall cross' pattern on SiO_2/Si substrates. We find that the electron transport in the printed MXene thin-film follows three-dimensional hopping according to the Mott variable range hopping (VRH) model. The WAL to WL crossover is seen in the magneto-conductance which we investigate over a range of (1.9 K to 50 K) with the WL/WAL crossover around 2.5 K to 3 K, indicating that the dominant charge transport mechanism changes at this temperature. We estimate a SOI field of H_{so} ~ 0.84 T and an inelastic field of H_i ~ 0.5 T at 1.9 K from the Maekawa-Fukuyama (MF) theory fitting.

2. Experimental

2.1 MXene synthesis

The synthesis of $Ti_3C_2T_x$ MXene begins with the production of the MAX phase. Ti_3AlC_2 MAX phase is produced by high-temperature annealing of three different powders (TiC (99.5%; Alfa Aesar, USA), Al (99.5%; Alfa Aesar, USA) and Ti (99.5%; Alfa Aesar, USA) mixed in an atomic ratio of 2:1:1). The precursor powder is ball milled at 60 rpm for 18 hours, then is annealed at 1400°C for 2 hours in a tube furnace in an Ar atmosphere. After cooling to room temperature, it is milled using a TiN-coated milling to convert the porous compact into a fine powder. The resultant Ti_3AlC_2 powder is passed through a 400-mesh sieve, leading to a final particle size that is below 37 μm. To selectively etch the Al layer of Ti_3AlC_2 MAX phase, Ti_3AlC_2 powder (50 g) is added in a mixed solution of HF, HCl, and H_2O (50 mL of HF; 49% by weight; Acros Organics), 300 mL of HCl (12M; Fisher Scientific; and 150 mL of H_2O) and stirring at 150 rpm for 24 hours at 35°C, as described in Ref. (Shuck *et al.* 2020). The etched mixture is rinsed repeatedly by centrifuging at 3,500 rpm in 10-minute cycles, decanting the clear acidic supernatant, and redispersing the powder in fresh deionized (DI) water until the pH of the supernatant is neutral (> 6 pH). To delaminate the multilayer of $Ti_3C_2T_x$, the etched powder is added to 1 L DI water and 50 g LiCl. This mixture is stirred in the reactor at 35°C for 24-h at 150 rpm. The $Ti_3C_2T_x$ is next washed with DI water by centrifugation at 3,500 rpm for 10 min in four 1 L centrifuge tubes. The supernatant is then decanted and the sediment redispersed in fresh DI water. This washing procedure is repeated until the supernatant is black (after 12 L total of DI water). The mixture is then centrifuged in 1-hour cycles, with the supernatant (clear) being decanted. This is repeated seven times (additional 28 L DI water). Following this, additional DI water is added, the mixture is centrifuged at 3,500 rpm for 10 minutes, and the dark supernatant is collected. This is repeated until the resultant supernatant was dilute (clear). This dark solution is collected and centrifuged at 3,500 rpm for an additional 10 min at 3,500 rpm to ensure no multilayer powder remains. The resulting solution is then concentrated by centrifugation at 10,000 rpm for 10 min. The concentrated sediment is redispersed in DI water to a final concentration to 30 mg/ml. In order to prepare an inkjet printable ink, DI water (1 ml) and ethanol (3 ml) are mixed with the $Ti_3C_2T_x$ mixture (1 g of the 30 mg/ml mixture), and sonicated for 10 minutes in a 20 kHz bath sonicator at 25°C. Following this, ethanol (20 ml) is added, and the mixture is sonicated for 30 min. The resultant metastable ink is centrifuged at 4,000 rpm for 60 min and the top 50% of centrifuged ink is collected for use.

2.2 Inkjet printing

For printing of the $Ti_3C_2T_x$ MXene thin film, a Dimatix DMP-2800 inkjet printer equipped with a 10 pL cartridge (DMC-11610) is used. 'Hall cross' patterns (see Fig. 1(a) and 1(d)) are inkjet printed with a drop spacing of 30 μm on

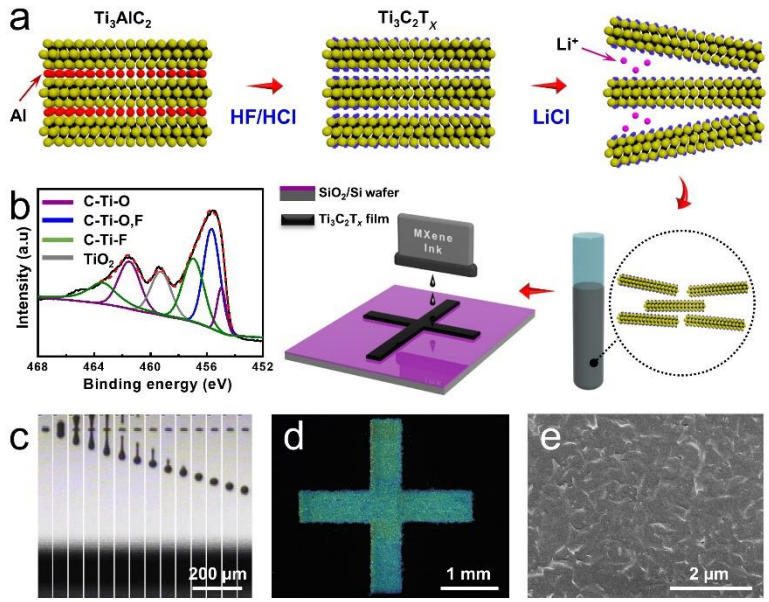

Fig. 1 Fabrication and characterization of the printed $Ti_3C_2T_x$ MXene thin-film. (a) Schematic diagrams of inkjet-printed $Ti_3C_2T_x$ MXene with cross-shaped (Hall cross) pattern. (b) High resolution XPS spectra of Ti 2p in $Ti_3C_2T_x$ MXene thin-film. (c) Sequential drop jetting of $Ti_3C_2T_x$ MXene ink. (d) Dark Field Optical microscopy image and (e) SEM micrograph of an inkjet-printed $Ti_3C_2T_x$ MXene thin-film surface

SiO_2 (100 nm)/Si and PET substrate at a substrate temperature of 60℃. For all the patterns, 15 print repetitions are used. After printing, the samples are kept at 60℃ for 5 minutes to ensure evaporation of the carrier solvents. The thickness of the printed $Ti_3C_2T_x$ thin-film is ~100 nm, and the length and width of each pattern line are 3 mm and 560 µm, respectively.

2.3 Measurements

The scanning electron microscope (SEM) micrograph in Fig. 1(e) was obtained using field-emission (S-4800, Hitachi). The XPS analysis (Fig. 1) is performed using a k-Alpha XPS system (Thermo Fisher Scientific) with a monochromatic Al Kα source (1486.6 eV). All electrical transport measurements are performed using a Quantum Design Physical Property Measurement System (PPMS, Quantum Design). Electrical contacts to Al pads and a puck are made with Ag paste and Cu wires. All electrical data are obtained using a Keithley 2636 sourcemeter and a Keithley 2182 nanovoltmeter.

3. Results and discussion

3.1 Basic properties of inkjet printed device

The MXene samples are synthesized from the Ti_3AlC_2 MAX phases, which are then formulated into inkjet printable inks to create the Hall-cross patterns on a 300 nm SiO_2/Si wafer (Fig. 1(a)). After ink formulation, we carry out XPS analysis of a MXene thin-film to confirm composition. Fig. 1(b) shows the deconvoluted peaks of Ti 2p from the XPS spectra, which correspond to the bonds of C-Ti-O (455.0 eV and 461.5 eV), C-Ti-O, F (455.7 eV), C-Ti-F (457.0 eV and 463.5 eV) and TiO_2 (459.3 eV). It is known that there is a mixture of −O, −OH, −Cl, and −F terminations on the flakes (Satheeshkumar *et al.* 2016, Shuck *et al.* 2020, 2019). The average lateral size of the flakes and average thickness in the prepared ink is 367 nm and 1.6 layers, respectively. The formulated ink carrier is based on a binary solvent mixture to enable reliable jetting and a uniform deposition onto the substrate as well as fast drying (Hu *et al.* 2018). Fig. 1(c) shows that the $Ti_3C_2T_x$ ink creates fine jetting during the printing process without forming unwanted satellite droplets. Fig. 1(d) shows a dark field image of a typical Hall Cross, each with line dimensions of 3 mm × 0.5 mm. The printed thin-film has a thickness of ~100 nm and appears uniform, with a heavily percolated/stacked structure. Although the edges of the printed structure are moderately sharp, we do not observe evidence for "coffee rings" (Hu *et al.* 2018, 2020) (i.e., strong deposition at the edges relative to the center; Fig. 1(d)).

3.2 Electrical transport model

The inkjet-printed Hall cross patterns of $Ti_3C_2T_x$ MXene sheets are then used to investigate the electronic transport behaviour versus temperature and magnetic field. A total of 15 Hall cross devices are printed onto SiO_2/Si wafers and PET substrate. The printed thin-film has a Hall mobility (μ_s) of 0.2 ~ 0.3 $cm^2 \cdot V^{-1} \cdot s^{-1}$ and a carrier concentration (n) in the 0.76 ~ 4.11 × 10^{23} cm^{-3} range. A typical temperature-dependent resistivity measurement for the Hall cross devices is shown in Fig. 2(a), exhibiting semiconductor behaviour with an exponential increase in resistivity with decreasing temperature.

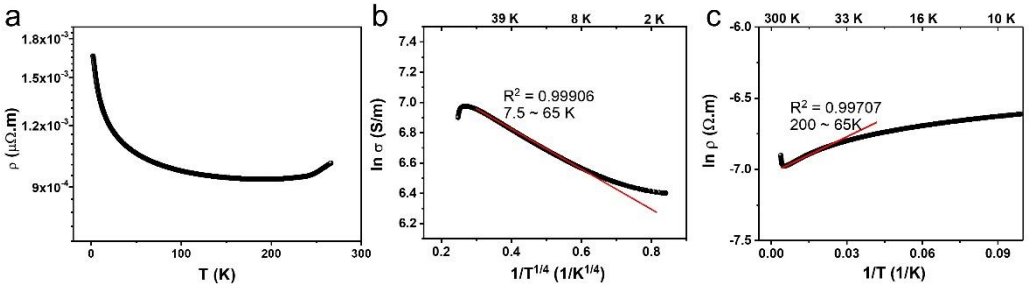

Fig. 2 Resistivity (ρ) and conductivity (σ) versus temperature (T). (a) ρ (T) showing a rise in ρ with decreasing T. (b) Ln(σ) versus $1/T^{1/4}$ for the inkjet-printed $Ti_3C_2T_x$ MXene network; the red line is a fit to the Mott VRH 3D model (with R^2 = 0.99906) in the low-T range (7.5 ~ 65 K). (c) ln σ versus $1/T$ for the inkjet-printed MXene network; the red line is a fit for the thermal activation model (with R^2 = 0.99707) at high T (200−65 K).

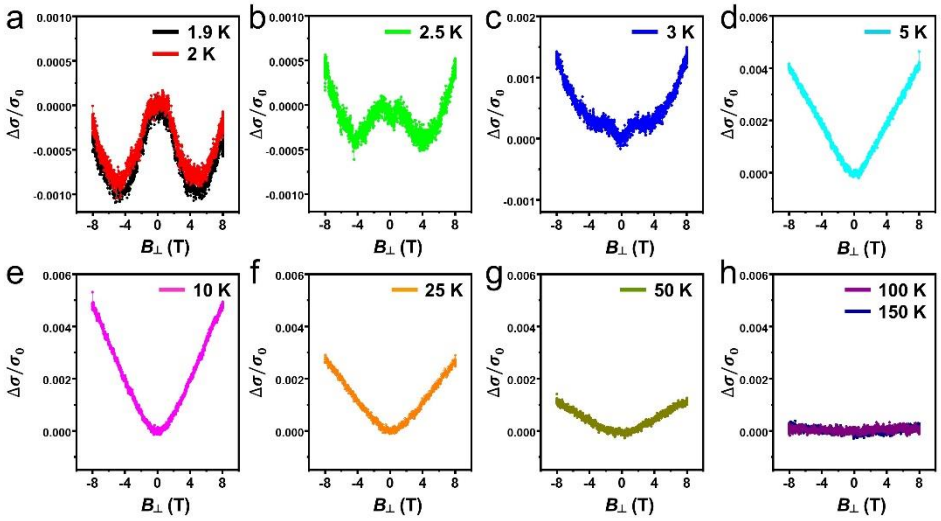

Fig. 3 Longitudinal magneto-conductance at different temperatures (labelled) with a perpendicular applied magnetic field. For 1.9 K (a) to 3 K (c), the WAL is decreased with a competing WL component. At 5 K (d), WAL cannot be distinguished from the magneto-conductance. For 10 K to 150 K (e-h), the total magneto-conductance ratio decreases with increasing temperature.

The VRH model is widely used to describe carrier transport in disordered semiconductors. Due to the random stacking of the nanosheets as shown in Fig. 1(e) and the presence of TiO_2 bonding as shown in Fig. 1(b), the printed $Ti_3C_2T_x$ MXene thin-film can be considered as a disordered system. We also argue that the presence of the edges in the MXene flakes additionally makes it a defect dominant system. Based on hopping theory, VRH has a dominant effect on electrical conductivity (σ) at low temperatures according to $\sigma = \sigma_0 \exp -(T_0/T)^x$ where σ_0 is the conductivity prefactor, T_0 is the characteristic temperature (Halim *et al.* 2016), and $x = (p + 1)/(d + p + 1)$ represents the relationship between the variation in the density of states at the Fermi level $D(E_F)$, p, and dimensionality of the material, d. Among the VRH models, the Mott VRH, which can be expressed as $\sigma = \sigma_0 \exp -\left(\frac{T_0}{T}\right)^{\frac{1}{4}}$ for 3-dimensional or $\sigma = \sigma_0 \exp -\left(\frac{T_0}{T}\right)^{\frac{1}{3}}$ for 2-dimensional cases describes low temperature conduction in strongly disordered systems with localized charge carrier states. We propose that this model explains the behaviour of the inkjet-printed $Ti_3C_2T_x$ thin-film in the low temperature regime since measurements show a $\ln\sigma - 1/T^{1/4}$ relationship from 7.5 K to 65 K. This follows a linear function with R^2 = 0.99906 from the linear fitting (Fig. 2(b)).

Above 65 K, thermal activation dominates the conductance and the nearest neighbor hopping (NNH) mechanism controls the electronic properties with $\sigma = \sigma_0 \exp -\left(\frac{E_a}{k_B T}\right)$, where E_a is the energy difference between the nearest localized states. The T-dependence of conductivity is fitted with $\ln\sigma - 1/T$ linear relationship (200 K ~ 65 K, R^2 = 0.99707) as shown in Fig. 2(c).

3.3 Low temperature electronic transport analysis - Localization

To investigate the charge carrier transport behaviour, we measured magnetoconductance between 1.9 K to 150 K; Fig. 3 shows magnetoconductance $\Delta\sigma$ / σ_0 = [σ (B) − σ (B=0)] / σ (B=0) versus an out-of-plane magnetic field ($B_\perp$). In the low temperature regime near 2 K (Fig. 3(a)), a large WAL is observed up to 4.5 T with a negative magneto-conductance. At 2.5 K, a small peak occurs near-zero

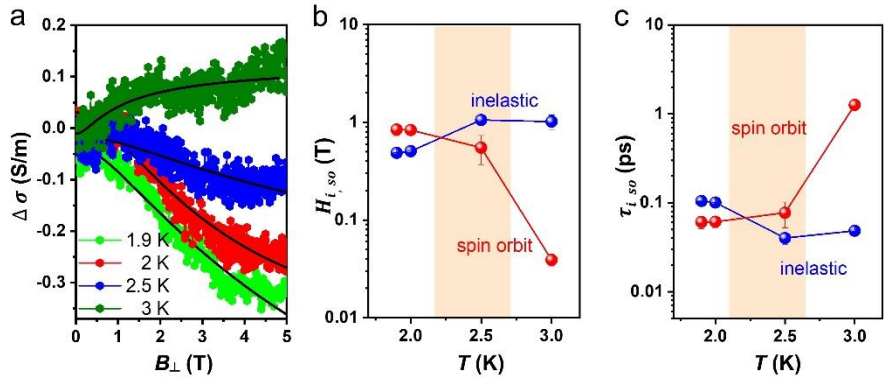

Fig. 4 Modulation of transport properties of printed $Ti_3C_2T_x$ MXene thin-film with an out-of-plane magnetic field ($B_\perp$). (a) $\Delta\sigma$ versus $B_\perp$ at different temperatures (different colors as labelled). Black lines are best fits from MF theory. (b) Obtained parameter $H_{i,}$ from the fitting using MF equations. (c) The extracted lifetimes (which correspond to the relaxation time) of $\tau_{i,\,so}$. The shaded region (b, c) indicates the WAL/WL crossover

magnetic field (Fig. 3(b)), consistent with competition between WAL and WL. This is likely due to strong SOI (Caviglia *et al.* 2014, Drouhin *et al.* 2014, Hansen *et al.* 2005, Kumar *et al.* 2015, Liu *et al.* 2012, Lu *et al.* 2015, Tikhonenko *et al.* 2009). As the temperature increases to 5 K (Figs. 3(c) and 3(d)), the negative magnetoconductance (which corresponds to WAL) disappears and only the positive WL regime remains. The WL magneto-conductance shows maximum signal at 10 K at up to 8 T (maximum field). When the temperature is further increased, the magneto-conductance signal slowly disappears around 100 K, likely due to thermal vibrations. This WAL/WL crossover is observed in all 15 samples regardless of the substrate. Similar results have previously been reported in other low dimensional/confined systems with disorder including $LaAl_xCr_{1-x}O_3/SrTiO_3$ 2D interfaces (Kumar *et al.* 2015), topological insulators (Liu *et al.* 2012), VSe_2 single crystals (Cao *et al.* 2017) and quantum wires (Hansen *et al.* 2005, Schäpers *et al.* 2006); the WAL/WL magneto-conductance crossover is observed in the printed $Ti_3C_2T_x$ thin-film, which is a defect-dominant system with strong disorder. We note that our printed thin-films, where the MXene nanosheets are randomly oriented, are different to those presented by Hamlin *et al.* which used $Ti_3C_2T_x$ multilayer structures (Halim *et al.* 2014).

The spin-orbit relaxation time is a key parameter to describe the WAL/WL crossover. The effect of SOI is analyzed from magnetoconductance in the diffusive transport regime which shows a strong dependence in the conductance variation ($\Delta\sigma$) on $B_\perp$; see Fig. 4(a). These results are modeled using the MF theory (Maekawa *et al.* 1981):

$$\Delta\sigma(H) = \frac{e^2}{\pi\hbar}\left[\Psi\left(\frac{H}{H_i + H_{so}}\right) + \frac{1}{2\sqrt{1-\Upsilon^2}}\Psi\left(\frac{H}{H_i + H_{so}\left(1+\sqrt{1-\Upsilon^2}\right)}\right) - \frac{1}{2\sqrt{1-\Upsilon^2}}\Psi\left(\frac{H}{H_i + H_{so}\left(1-\sqrt{1-\Upsilon^2}\right)}\right)\right] \quad (1)$$

where $\Psi(x) = \ln(x) + \psi(1/2 + 1/x)$ with $\psi(x)$ a digamma function H_i and H_{so} are the inelastic and spin-orbit fields, which relate to the inelastic time (τ_i) and spin-orbit time (τ_{so}) *via* $H_{i,so} = \hbar/4eD\tau_{i,so}$. The Zeeman correction of Υ is expressed as $\Upsilon = g\mu_B H/4eDH_{so}$ using the electron g factor and Bohr magneton (μ_B). The fits to $\Delta\sigma$ ($B_\perp$) in Fig. 4(a) are conducted up to 5 T considering the critical field and diffusive transport regime of electrons (Datta 1995, Heikkilä *et al.* 2013).

For the fitting analysis, we use σ_0 as a prefactor in order to include some additional carrier movement such as flake to flake transport and grain boundary transport. From these fits, we can extract $H_{i,so}$ close to the temperature regime of WAL/WL. For the range of fields and temperature analyzed, the observed WAL/WL crossover is in agreement (in Fig. 4(b)) between the spin-orbit and inelastic scattering fields (with parameters $H_{i,so}$). For the WAL dominant temperature of 1.9 K and 2 K, SOI field H_{so} shows a maximum value of 0.85 T, which is higher than the inelastic field of H_i ~ 0.5 T. When the temperature is increased over 2.5 K, H_{so} is dramatically decreased by more than one order of magnitude resulting in $H_{so} \ll H_i$. Thus, WAL diminishes with increasing temperature further.

We note that this is the first observation of a wide WAL/WL crossover of printed $Ti_3C_2T_x$ MXene thin-film and the high magnitude of H_{so} at very low temperature is unique. Our analysis gives a relatively high value of H_{so} ~ 0.85 T at 1.9 K, and indicates strong SOI in the printed MXene thin-film compared with other material systems such as 2D scale Tellurium (H_{so} ~ 0.09 T at 1 K) (Niu *et al.* 2020), few-layered VSe_2 (H_{so} ~ 0.7 T at 2 K) (Liu *et al.* 2019), bulk Bi_2Te_3 (H_{so} ~ 0.92 T at 2 K) (Dey *et al.* 2014), and quasi-2D $LaAlO_3/EuTiO_3/SrTiO_3$ system (H_{so} ~ 1.0 T at 2 K) (Stornaiuolo *et al.* 2018). For comparison, we plotted H_{so} is the low temperature regime with various material systems including bulk, 2-dimensional (2D), and thin films (Fig. 5).

From the $H_{i,so}$ parameters obtained from our fitting analysis (Fig. 4(a)), we have determined the relaxation time $\tau_{i,so}$ *via* $D = v_F^2\tau/2$ to estimate the diffusion constant D. From estimates of Fermi velocity and elastic scattering time using a parabolic dispersion relation with a fixed effective mass m^*, we are able to estimate the diffusion coefficient

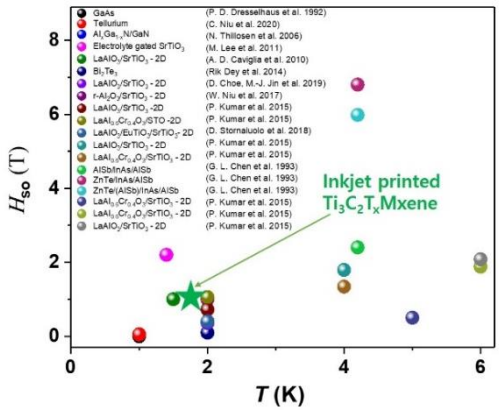

Fig. 5 H_{so} for different materials and structures (labels) versus temperature (T).

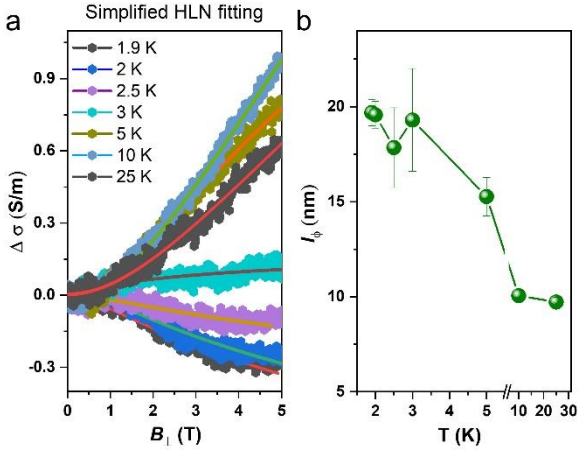

Fig. 6 Simplified HLN fitting (a) fitted curve (linear curve) and the original data (dotted curve) (b) extracted phase coherence length l_ϕ as a function of temperature.

using $m^* = 0.5\ m_e$ (where m_e is the free electron mass) (Hu *et al.* 2015). The estimated relaxation times are plotted in Fig. 4(c). The temperature range which we implement fitting analysis shows that the change in inelastic scattering time remains relatively small (~ 0.1 ps), whereas the spin-orbit scattering time has a relatively large variation (increasing up to 1.26 ps at 3 K). For temperatures below the WAL/WL crossover, we observe that the inelastic scattering time is longer than the spin-orbit scattering time (spin relaxation time). This indicates that the effect of SOI is strong compared to the orbital effect of the applied magnetic field. Above the crossover temperature (> 2 K), the SOI scattering time is dramatically increased compared to the inelastic scattering time. This means that the SOI is weaker with increasing temperatures above 2.5 K. In contrast, the inelastic scattering time remains almost constant over this temperature regime. A similar type of WAL/WL crossover behaviour with increasing temperature has been reported before in low bandgap single crystal semiconductors in the mT magnetic field range (Hansen *et al.* 2005, Schäpers *et al.* 2006). However, such a WAL/WL crossover in highly disordered and defect dominant systems such as inkjet-printed $Ti_3C_2T_x$ MXene thin-film has not been reported to our knowledge. Furthermore, this type of WAL/WL crossover behaviour is observed under a wider magnetic field (± 4T) variation compared with other materials previously reported (Hansen *et al.* 2005, Schäpers *et al.* 2006). Individual MXene nanosheets have defects and disorder with electron spin currents along the Hall cross bars interacting with individual MXene nanosheets meaning that sheet-to-sheet transport will alter quantum mechanical transport. Furthermore, the nanosheets are strained and contain impurities, vacancies, and oxidized regions. We can thus assume that the majority of the WL magneto-conductance behaviour results from strong disorder of the nanosheet inkjet printed system and the high SOI will produce strong WAL magneto-conductance due to the breaking of time reversal symmetry at low temperature.

To understand further the magneto-conductance trend as a function of temperature, the simplified Hikami-Larkin-Nagaoka (HLN) theory (Datta 1995, Dey *et al.* 2014, Hikami *et al.* 1980) has also used to fit the experimental data (Fig. 6) in terms of variation of conductance Δσ (B) = σ (B) - σ (0) as shown below (Liu *et al.* 2012),

$$\Delta\sigma(B) = \frac{\alpha e^2}{2\pi^2\hbar}\left[\psi\left(\frac{1}{2}+\frac{\hbar}{4eBl_\phi}\right) - \ln\left(\frac{\hbar}{4eBl_\phi}\right)\right], \qquad (2)$$

where $\psi(x)$ is the digamma function, l_ϕ and α are the phase coherence length and a coefficient indicating the type of localization, respectively. From our fitting, l_ϕ gradually decreases with increasing temperature as shown in Fig. 6(b).

The extracted value of α can be used to determine material state which can be distinguished with orthogonal ($\alpha = 1$), unitary ($\alpha = 0$), and simpletic ($\alpha = 0.5$) cases, respectively (Lang *et al.* 2013): $\alpha = 1$ corresponds to elastic state which have two channels of thicker films, rather than simpletic represents single channel with WAL ($\alpha = -0.5$) or WL ($\alpha = +0.5$); and unitary is the case of magnetic (Hikami *et al.* 1980, Lang *et al.* 2013).

This simplified HLN theory is based on the low dimensional transport analysis. In our system, the magneto-conductance behaviour is well fitted with the simplified HLN equation and we expected the coefficient α to be ±0.5 although we obtain a much higher value of several orders of magnitude. This result may be due to the complex structure of the inkjet-printed MXene thin-film which has a high defect concentration and a relatively high thickness (100 nm). However, the trend of α is negative up to 2.5 K, then changes to positive from 3 K, matching the WAL/WL crossover temperature. Furthermore, we estimate the temperature-dependence of l_ϕ, which reaches a maximum ($l_\phi \sim 20$ nm) at near 2 K and gradually decreases with increasing temperature up to 25 K ($l_\phi \sim 10$ nm).

3.4 Low temperature electronic transport analysis - Localization

To confirm that the WAL/WL crossover is substrate-independent, matching $Ti_3C_2T_x$ MXene Hall cross networks are fabricated on uncoated PET substrates. These show similar magneto-conductance behaviour in the2 K to 50 K range (Fig. 7) as the thin-films on SiO_2/Si. The WAL/WL crossover on PET is near 2 K in agreement with the inflexible substrates (Fig. 3).

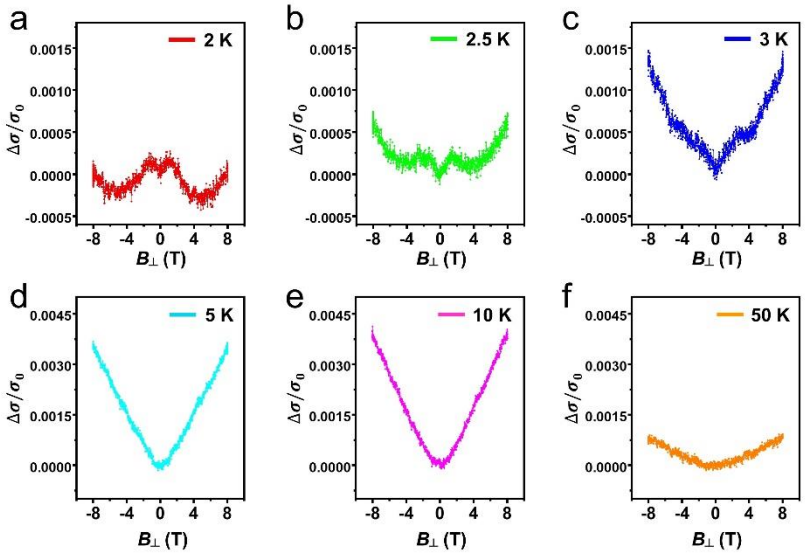

Fig. 7 Magneto-conductance of inkjet-printed $Ti_3C_2T_x$ MXene network on flexible PET substrates with a perpendicular applied magnetic field $B_\perp$. With increasing temperature from 2 K (a) – 50 K (f), WAL/WL is visible at 2.5 K

4. Conclusions

We have investigated the electronic transport of inkjet printed $Ti_3C_2T_x$ MXene thin-film Hall cross devices. A WAL/WL magneto-conductance crossover in the thin-films is observed between 2.5 K to 3 K, consistent with strong SOI below 3 K. By analyzing the magneto-conductance using the MF theory, we obtain a spin-orbit field H_{so} of ~ 0.84 T and an inelastic field H_i of ~ 0.5 T at 1.9 K. Our results are of interest for potential applications of printed MXene thin-film in flexible spintronic/spin-orbitronic devices where SOI is fundamental for spin transport control. Our results and analyses offer a deeper insight into microscopic charge carrier transport inkjet printed $Ti_3C_2T_x$, showing promising properties for printed electronic flexible and smart device applications.

Acknowledgments

This work was supported by the Institute for Basic Science (IBS-R019-Y1) and the National Research Foundation of Korea (NRF) grant funded by the Korea government (2021M3H4A1A02050421). J. W. A. R. acknowledges funding from the EPSRC through the EPSRC-JSPS Core-to-Core Grant "Oxide Superspin" (EP/P026311/1). We are grateful to Prof. Gogotsi's group (including Kathleen Maleski, Kanit Hantanasirisakul, Christopher E. Shuck, and Prof. Yury Gogotsi at Drexel University) for their supporting the Ti_3C_2 MXene materials and to Prof. Hassan's group (including Shouhu Liu, Guohua Hu, and Prof. Tawfique Hasan at University of Cambridge) for their supporting the inkjet printing.

References

Akuzum, B., Maleski, K., Anasori, B., Lelyukh, P., Alvarez, N.J., Kumbur, E.C. and Gogotsi, Y. (2018), "Rheological characteristics of 2D titanium carbide (MXene) dispersions: A guide for processing MXenes", *ACS Nano*, **12**(3), 2685-2694. https://doi.org/10.1021/acsnano.7b08889.

Anasori, B., Lukatskaya, M.R. and Gogotsi, Y. (2017), "2D metal carbides and nitrides (MXenes) for energy storage", *Nat. Rev. Mater.*, **2**(2), 1-17. https://doi.org/10.1038/natrevmats.2016.98.

Anasori, B., Shi, C., Moon, E.J., Xie, Y., Voigt, C.A., Kent, P.R.C., May, S.J., Billinge, S.J.L., Barsoum, M.W. and Gogotsi, Y. (2016), "Control of electronic properties of 2D carbides (MXenes) by manipulating their transition metal layers", *Nanosc. Horiz.*, **1**(3), 227-234. https://doi.org/10.1039/C5NH00125K.

Anasori, B., Xie, Y., Beidaghi, M., Lu, J., Hosler, B.C., Hultman, L., Kent, P.R.C., Gogotsi, Y. and Barsoum, M.W. (2015), "Two-dimensional, ordered, double transition metals carbides (MXenes)", *ACS Nano*, **9**(10), 9507-9516. https://doi.org/10.1021/acsnano.5b03591.

Cao, Q., Yun, F. F., Sang, L., Xiang, F., Liu, G. and Wang, X. (2017), "Defect introduced paramagnetism and weak localization in two-dimensional metal VSe_2", *Nanotechnology*, **28**(47), 475703. https://doi.org/10.1088/1361-6528/aa8f6c.

Caviglia, A.D., Gabay, M., Gariglio, S., Reyren, N., Cancellieri, C. and Triscone, J.M. (2014), "Tunable rashba spin-orbit interaction at oxide interfaces", *Phys. Rev. Lett.*, **104**(12), 126803. https://doi.org/10.1103/PhysRevLett.104.126803.

Chandrasekaran, A., Mishra, A. and Singh, A.K. (2017), "Ferroelectricity, antiferroelectricity, and ultrathin 2D electron/hole gas in multifunctional monolayer MXene", *Nano Lett.*, **17**(5), 3290-3296. https://doi.org/10.1021/acs.nanolett.7b01035.

Dahlqvist, M. and Rosen, J. (2020), "Predictive theoretical screening of phase stability for chemical order and disorder in quaternary 312 and 413 MAX phases", *Nanoscale*, **12**(2), 785-794. https://doi.org/10.1039/C9NR08675G.

Datta, S. (1995), *Electronic Transport in Mesoscopic Systems*, Cambridge University Press, 196-245.

Dey, R., Pramanik, T., Roy, A., Rai, A., Guchhait, S., Sonde, S., Movva, H.C.P., Colombo, L., Register, L.F. and Banerjee, S.K. (2014), "Strong spin-orbit coupling and Zeeman spin splitting in angle dependent magnetoresistance of Bi_2Te_3", *Appl. Phys. Lett.*, **104**(22), 223111. https://doi.org/10.1063/1.4881721.

Deysher, G., Shuck, C.E., Hantanasirisakul, K., Frey, N.C.,

Foucher, A.C., Maleski, K., Sarycheva, A., Shenoy, V.B., Stach, E.A., Anasori, B. and Gogotsi, Y. (2020), "Synthesis of Mo_4VAlC_4 MAX phase and two-dimensional Mo_4VC_4 MXene with five atomic layers of transition metals", *ACS Nano*, **14**(1), 204-217. https://doi.org/10.1021/acsnano.9b07708.

Dresselhaus, P.D., Papavassiliou, C.M.A., Wheeler, R.G. and Sacks, R.N. (1992), "Observation of spin precession in GaAs inversion layers using antilocalization", *Phys. Rev. Lett.*, **68**(1), 106-109. https://doi.org/10.1103/PhysRevLett.68.106.

Drouhin, H.J., Wegrowe, J.E., Razeghi, M., Lu, H.Z. and Shen, S.Q. (2014), "Weak localization and weak anti-localization in topological insulators", *Proc. SPIE*, **9167**, 91672E. https://doi.org/10.1117/12.2063426.

Enyashin, A.N. and Ivanovskii, A.L. (2012), "Atomic structure, comparative stability and electronic properties of hydroxylated Ti_2C and Ti_3C_2 nanotubes", *Comput. Theor. Chem.*, **989**, 27-32. https://doi.org/10.1016/j.comptc.2012.02.034.

Fashandi, H., Ivády, V., Eklund, P., Spetz, A.L., Katsnelson, M.I. and Abrikosov, I.A. (2015), "Dirac points with giant spin-orbit splitting in the electronic structure of two-dimensional transition-metal carbides", *Phys. Rev. B*, **92**(15), 155142. https://doi.org/10.1103/PhysRevB.92.155142.

Gao, G., Ding, G., Li, J., Yao, K., Wu, M. and Qian, M. (2016), "Monolayer MXenes: Promising half-metals and spin gapless semiconductors", *Nanoscale*, **8** (16), 8986-8994. https://doi.org/10.1039/C6NR01333C.

Ghidiu, M., Lukatskaya, M.R., Zhao, M.Q., Gogotsi, Y. and Barsoum, M.W. (2014), "Conductive two-dimensional titanium carbide 'clay' with high volumetric capacitance", *Nature*, **516**(7529), 78-81.

Guo, D., Ming, F., Su, H., Wu, Y., Wahyudi, W., Li, M., Hedhili, M.N., Sheng, G., Li, L.J., Alshareef, H.N., Li, Y. and Lai, Z. (2019), "MXene based self-assembled cathode and antifouling separator for high-rate and dendrite-inhibited Li–S battery", *Nano Energy*, **61**, 478-485. https://doi.org/10.1016/j.nanoen.2019.05.011.

Halim, J., Lukatskaya, M.R., Cook, K.M., Lu, J., Smith, C.R., Näslund, L.Å., May, S.J., Hultman, L. Gogotsi, Y., Eklund, P. and Barsoum, M.W. (2014), "Transparent conductive two-dimensional titanium carbide epitaxial thin films", *Chem. Mater*, **26**(7), 2374-2381. https://doi.org/10.1021/cm500641a

Halim, J., Kota, S., Lukatskaya, M.R., Naguib, M., Zhao, M.Q., Moon, E.J., Pitock, J., Nanda, J., May, S.J., Gogotsi, Y. and Barsoum, M.W. (2016), "Synthesis and characterization of 2D molybdenum carbide (MXene)", *Adv. Func. Mater.*, **26**(18), 3118-3127. https://doi.org/10.1002/adfm.201505328.

Halim, J., Moon, E.J., Eklund, P., Rosen, J., Barsoum, M.W. and Ouisse, T. (2018), "Variable range hopping and thermally activated transport in molybdenum-based MXenes", *Phys. Rev. B*, **98** (10), 104202. https://doi.org/10.1103/PhysRevB.98.104202.

Halim, J., Persson, I., Moon, E.J., Kuhne, P., Darakchieva, V., Persson, P.O.A., Eklund, P., Rosen, J. and Barsoum, M.W. (2019), "Electronic and optical characterization of 2D Ti_2C and Nb_2C (MXene) thin films", *J. Phys. Condens. Matter.*, **31** (16), 165301. https://doi.org/10.1088/1361-648X/ab00a2.

Han, M., Shuck, C.E., Rakhmanov, R., Parchment, D., Anasori, B., Koo, C.M., Friedman, G. and Gogotsi, Y. (2020), "Beyond $Ti_3C_2T_X$: MXenes for electromagnetic interference shielding", *ACS Nano*, **14** (4), 5008-5016. https://doi.org/10.1021/acsnano.0c01312.

Hansen, A.E., Björk, M.T., Fasth, C., Thelander, C. and Samuelson, L. (2005), "Spin relaxation in InAs nanowires studied by tunable weak antilocalization", *Phys. Rev. B*, **71**(20), 205328. https://doi.org/10.1103/PhysRevB.71.205328.

Heikkilä, T.T. (2013), *The Physics of Nanoelectronics: Tansport and Fluctuation Phenomena at Low Temperatures*, Oxford University Press, 296.

Hikami, S., Larkin, A.I., Nagaoka, Y. (1980), "Spin-orbit interaction and magnetoresistance in the two dimensional random system", *Prog. Theor. Phys.*, **63**(2), 707-710. https://doi.org/10.1143/PTP.63.707.

Hu, T., Zhang, H., Wang, J., Li, Z., Hu, M., Tan, J., Hou, P., Li, F. and Wang, X. (2015), "Anisotropic electronic conduction in stacked two-dimensional titanium carbide", *Sci. Rep.*, **5**, 16329. https://doi.org/10.1038/srep16329.

Hu, G., Kang, J., Ng, L. W.T., Zhu, X., Howe, R.C.T., Jones, C.G., Hersam, M.C. and Hasan, T. (2018), "Functional inks and printing of two-dimensional materials", *Chem. Soc. Rev.*, **47** (9), 3265-3300. https://doi.org/10.1039/C8CS00084K.

Hu, G., Yang, L., Yang, Z., Wang, Y., Jin, X., Dai, J., Wu, Q., Liu, S., Zhu, X., Wang, X., Wu, T.C, Howe, R.C.T., Albow-Owen, T., Ng, L.W.T., Yang, Q., Occhipinti, L.G., Woodward, R.I., Kelleher, E.J.R., Sun, Z., Huang, X., Zhang, M., Bain, C.D. and Hasan, T. (2020), "A general ink formulation of 2D crystals for wafer-scale inkjet printing", *Sci. Adv.*, **6**, eaba5029. https://doi.org/10.1126/sciadv.aba5029.

Jiang, X., Kuklin, A.V., Baev, A., Ge, Y., Ågren, H., Zhang, H. and Prasad, P.N. (2020), "Two-dimensional MXenes: From morphological to optical, electric, and magnetic properties and applications", *Phys. Rep.*, **848**, 1-58. https://doi.org/10.1016/j.physrep.2019.12.006.

Khazaei, M., Arai, M., Sasaki, T., Chung, C.Y., Venkataramanan, N.S., Estili, M., Sakka, Y. and Kawazoe, Y. (2013), "Novel electronic and magnetic properties of two-dimensional transition metal carbides and nitrides", *Adv. Func. Mater.*, **23**(17), 2185-2192. https://doi.org/10.1002/adfm.201202502.

Khazaei, M., Ranjbar, A., Arai, M. and Yunoki, S. (2016), "Topological insulators in the ordered double transition metals M′2M″C2 MXenes (M′= Mo, W; M″=Ti, Zr, Hf)", *Phys. Rev. B*, **94**(12), 125152. https://doi.org/10.1103/PhysRevB.94.125152.

Khazaei, M., Ranjbar, A., Arai, M., Sasaki, T. and Yunoki, S. (2017), "Electronic properties and applications of MXenes: A theoretical review", *J. Mater. Chem. C*, **5**(10), 2488-2503. https://doi.org/10.1039/C7TC00140A.

Kumar, H., Frey, N.C., Dong, L., Anasori, B., Gogotsi, Y. and Shenoy, V.B. (2017), "Tunable magnetism and transport properties in nitride MXenes", *ACS Nano*, **11**(8), 7648-7655. https://doi.org/10.1021/acsnano.7b02578.

Kumar, P., Dogra, A., Bhadauria, P.P., Gupta, A., Maurya, K.K. and Budhani, R.C. (2015), "Enhanced spin–orbit coupling and charge carrier density suppression in $LaAl_{1-x}Cr_xO_3/SrTiO_3$ hetero-interfaces", *J. Phys. Condens. Matter.*, **27** (12), 125007. https://doi.org/10.1088/0953-8984/27/12/125007.

Lane, N.J., Barsoum, M.W. and Rondinelli, J.M. (2013), "Correlation effects and spin-orbit interactions in two-dimensional hexagonal 5d transition metal carbides, $Ta_{n+1}C_n$ (n = 1,2,3)", *EPL*, **101**(5), 57004. https://doi.org/10.1209/0295-5075/101/57004.

Lang, M., He, L., Kou, X., Upadhyaya, P., Fan, Y., Chu, H., Jiang, Y., Bardarson, J.H., Jiang, W., Choi, E.S., Wang, Y., Yeh, N.C. Moore, J., Wang, K.L. (2013), "Competing weak localization and weak antilocalization in ultrathin topological insulators", *Nano Lett.*, **13**(1), 48-53. https://doi.org/10.1021/nl303424n.

Lee, M., Williams, J.R., Zhang, S., Frisbie, C.D. and Goldhaber-Gordon, D. (2011), "Electrolyte gate-controlled Kondo effect in $SrTiO_3$", *Phys. Rev. Lett.*, **107**(25), 256601. https://doi.org/10.1103/PhysRevLett.107.256601.

Liu, H., Bao, L., Zhou, Z., Che, B., Zhang, R., Bian, C., Ma, R., Wu, L., Yang, H., Li, J., Gu, C., Shen, C.M., Du, S. and Gao, H.J. (2019), "Quasi-2D transport and weak antilocalization effect in few-layered VSe_2", *Nano Lett.*, **19**(7), 4551-4559. https://doi.org/10.1021/acs.nanolett.9b01412.

Liu, L., Ying, G., Wen, D., Hu, C., Zhang, C. and Wang, C. (2021),

"Strengthening effect of $Ti_3C_2T_X$ in copper matrix composites prepared by molecular-level and high-shear mixings and SPS", *Adv. Nano. Res.*, **11**(3), 271-280. https://doi.org/10.12989/anr.2021.11.3.271.

Liu, M., Zhang, J., Chang, C.Z., Zhang, Z., Feng, X., Li, K., He, K., Wang, L.L., Chen, X., Dai, X., Fang, Z., Xue, Q. K., Ma, X. and Wang, Y. (2012), "Crossover between weak antilocalization and weak localization in a magnetically doped topological insulator", *Phys. Rev. Lett.*, **108**(3), 036805. https://doi.org/10.1103/PhysRevLett.108.036805.

Liu, W.E., Hankiewicz, E.M. and Culcer, D. (2017), "Weak localization and antilocalization in topological materials with impurity spin-orbit interactions", *Materials*, **10**(7), 807. https://doi.org/10.3390/ma10070807.

Lu, H.Z. and Shen, S.Q. (2015), "Weak antilocalization and localization in disordered and interacting Weyl semimetals", *Phys. Rev. B*, **92**(3), 035203. https://doi.org/10.1103/PhysRevB.92.035203.

Maekawa, S., Fukuyama, H. (1981), "Magnetoresistance in two-dimensional disordered systems: Effects of zeeman splitting and spin-orbit scattering", *J. Phys. Soc. Jap.*, **50**(8), 2516-2524. https://doi.org/10.1143/JPSJ.50.2516.

Maleski, K., Mochalin, V. N. and Gogotsi, Y. (2017), "Dispersions of two-dimensional titanium carbide mxene in organic solvents", *Chem. Mater.*, **29**(4), 1632-1640. https://doi.org/10.1021/acs.chemmater.6b04830.

Naguib, M., Kurtoglu, M., Presser, V., Lu, J., Niu, J., Heon, M., Hultman, L., Gogotsi, Y. and Barsoum, M.W. (2011), "Two-dimensional nanocrystals produced by exfoliation of Ti_3AlC_2", *Adv. Mater.*, **23** (37), 4248-53. https://doi.org/10.1002/adma.201102306.

Naguib, M., Mashtalir, O., Carle, J., Presser, V., Lu, J., Hultman, L., Gogotsi, Y. and Barsoum, M.W. (2012), "Two-dimensional transition metal carbides", *ACS Nano*, **6** (2), 1322-1331. https://doi.org/10.1021/nn204153h.

Niu, C., Qiu, G., Wang, Y., Zhang, Z., Si, M., Wu, W. and Ye, P.D. (2020), "Gate-tunable strong spin-orbit interaction in two-dimensional tellurium probed by weak antilocalization", *Phys. Rev. B*, **101** (20), 205414. https://doi.org/10.1103/PhysRevB.101.205414.

Pinto, D., Anasori, B., Avireddy, H., Shuck, C.E., Hantanasirisakul, K., Deysher, G., Morante, J.R., Porzio, W., Alshareef, H.N. and Gogotsi, Y. (2020), "Synthesis and electrochemical properties of 2D molybdenum vanadium carbides – solid solution MXenes", *J. Mater. Chem. A*, **8**(18), 8957-8968. https://doi.org/10.1039/D0TA01798A.

Salles, P., Pinto, D., Hantanasirisakul, K., Maleski, K., Shuck, C. E. and Gogotsi, Y. (2019), "Electrochromic effect in titanium carbide mxene thin films produced by dip-coating", *Adv. Func. Mater.*, **29** (17), 1809223. https://doi.org/10.1002/adfm.201809223.

Sarycheva, A., Polemi, A., Liu, Y., Dandekar, K., Anasori, B. and Gogotsi, Y. (2018), "2D titanium carbide (MXene) for wireless communication", *Sci. Adv.*, **4** (9), eaau0920. https://www.science.org/doi/10.1126/sciadv.aau0920.

Satheeshkumar, E., Makaryan, T., Melikyan, A., Minassian, H., Gogotsi, Y. and Yoshimura, M. (2016), "One-step solution processing of Ag, Au and Pd@MXene Hybrids for SERS", *Sci. Rep.*, **6**, 32049. https://doi.org/10.1038/srep32049.

Schäpers, T., Guzenko, V.A., Pala, M.G., Zülicke, U., Governale, M., Knobbe, J. and Hardtdegen, H. (2006), "Suppression of weak antilocalization in $Ga_xIn_{1-x}As$ / InP narrow quantum wires", *Phys. Rev. B*, **74**(8), 081301(R). https://doi.org/10.1103/PhysRevB.74.081301.

Schmidt, H., Yudhistira, I., Chu, L., Castro Neto, A. H., Özyilmaz, B., Adam, S. and Eda, G. (2016), "Quantum Transport and Observation of Dyakonov-Perel Spin-Orbit Scattering in Monolayer MoS_2", *Phys. Rev. Lett.*, **116**(4), 046803. https://doi.org/10.1103/PhysRevLett.116.046803.

Shuck, C.E., Han, M., Maleski, K., Hantanasirisakul, K., Kim, S. J., Choi, J., Reil, W.E.B. and Gogotsi, Y. (2019), "Effect of Ti_3AlC_2 MAX Phase on Structure and Properties of Resultant $Ti_3C_2T_X$ MXene", *ACS Appl. Nano Mater.*, **2**(6), 3368-3376. https://doi.org/10.1021/acsanm.9b00286.

Shuck, C.E., Sarycheva, A., Anayee, M., Levitt, A., Zhu, Y., Uzun, S., Balitskiy, V., Zahorodna, V., Gogotsi, O. and Gogotsi, Y. (2020), "Scalable Synthesis of $Ti_3C_2T_X$ MXene", *Adv. Eng. Mater.*, **22**(3). https://doi.org/10.1002/adem.201901241.

Si, C., Zhou, J. and Sun, Z. (2015), "Half-metallic ferromagnetism and surface functionalization-induced metal–insulator transition in graphene-like two-dimensional Cr_2C crystals", *ACS Appl. Mater. Inter.*, **7**(31), 17510-5. https://doi.org/10.1021/acsami.5b05401.

Soundiraraju, B. and George, B.K. (2017), "Two-dimensional titanium nitride (ti_2n) mxene: Synthesis, characterization, and potential application as surface-enhanced raman scattering substrate", *ACS Nano*, **11**(9), 8892-8900. https://doi.org/10.1021/acsnano.7b03129.

Stornaiuolo, D., Jouault, B., Di Gennaro, E., Sambri, A., D'Antuono, M., Massarotti, D., Granozio, F.M., Di Capua, R., De Luca, G.M., Pepe, G.P., Tafuri, F. and Salluzzo, M. (2018), "Interplay between spin-orbit coupling and ferromagnetism in magnetotransport properties of a spin-polarized oxide two-dimensional electron system", *Phys. Rev. B*, **98**(7), 075409. https://doi.org/10.1103/PhysRevB.98.075409.

Tikhonenko, F.V., Kozikov, A.A., Savchenko, A.K. and Gorbachev, R.V. (2009), "Transition between electron localization and antilocalization in graphene", *Phys. Rev. Lett.*, **103**(22), 226801. https://doi.org/10.1103/PhysRevLett.103.226801.

Urbankowski, P., Anasori, B., Makaryan, T., Er, D., Kota, S., Walsh, P.L., Zhao, M., Shenoy, V.B., Barsoum, M.W. and Gogotsi, Y. (2016), "Synthesis of two-dimensional titanium nitride Ti_4N_3 (MXene)", *Nanoscale*, **8** (22), 11385-11391. https://doi.org/10.1039/C6NR02253G.

VahidMohammadi, A., Rosen, J. and Gogotsi, Y. (2021), "The world of two-dimensional carbides and nitrides (MXenes)", *Science*, **372**, 1165. https://doi.org/10.1126/science.abf1581.

Weng, H., Ranjbar, A., Liang, Y., Song, Z., Khazaei, M., Yunoki, S., Arai, M., Kawazoe, Y., Fang, Z. and Dai, X. (2015), "Large-gap two-dimensional topological insulator in oxygen functionalized MXene", *Phys. Rev. B*, **92**(7), 075436. https://doi.org/10.1103/PhysRevB.92.075436.

Xie, Y. and Kent, P.R.C. (2013), "Hybrid density functional study of structural and electronic properties of functionalized $Ti_{n+1}X_n$ (X=C, N) monolayers", *Phys. Rev. B*, **87**(23), 235441. https://doi.org/10.1103/PhysRevB.87.235441.

Zha, X.H., Luo, K., Li, Q., Huang, Q., He, J., Wen, X. and Du, S. (2015), "Role of the surface effect on the structural, electronic and mechanical properties of the carbide MXenes", *EPL*, **111**(2), 26007. https://doi.org/10.1209/0295-5075/111/26007.

JL